Vibrational wave packets in the $B\,^1\Pi_u$ and $D\,^1\Sigma_u^+$ states of Cs_2: Determination of improved $Cs_2^+(X)$ and $Cs_2(B)$ spectroscopic constants

A. L. Oldenburg, P. C. John,[a] and J. G. Eden
Laboratory for Optical Physics and Engineering, Department of Electrical and Computer Engineering, University of Illinois, Urbana, Illinois 61801

(Received 13 July 2000; accepted 26 September 2000)

Vibrational wave packets in the $B\,^1\Pi_u$ and $D\,^1\Sigma_u^+$ excited states of Cs_2 have been studied on the ~100 fs time scale by pump–probe laser spectroscopy. The temporal behavior of the wave packets was monitored by photoionizing the electronically excited molecule with a time-delayed probe pulse and recording the time and energy-integrated photoelectron signal as a function of time delay between the pump and probe pulses. For the $B\,^1\Sigma_u^+$ experiments, wave packets were produced by exciting the $B\,^1\Sigma_u^+ \leftarrow X\,^1\Sigma_g^+$ transition in the ~740–790 nm region and subsequently detected by photoionizing the molecule at wavelengths between 565 nm and 600 nm. By simulating the experimentally observed transients with the density matrix formalism (and explicitly accounting for laser chirp and $|\Delta v|>1$ coherences), improved values for the equilibrium internuclear separation for the $Cs_2(B\,^1\Pi_u)$ state and T_e for the $Cs_2^+(X)$ state were determined to be $R_e(B\,^1\Pi_u)=4.93\pm0.03$ Å and $T_e[Cs_2^+(X)]=29\,930\pm100\,cm^{-1}$, respectively. Similar experiments were conducted for the $D\,^1\Sigma_u^+$ state. Wave packets composed of vibrational levels ($v'\approx40-50$) perturbed by the bound $2\,^3\Pi_{ou}$ state were produced on the $D\,^1\Sigma_u^+$ potential surface by driving the $D\,^1\Sigma_u^+ \leftarrow X\,^1\Sigma_g^+$ transition in the 575–610 nm spectral interval. © *2000 American Institute of Physics.* [S0021-9606(00)00248-8]

I. INTRODUCTION

The temporal dynamics of vibrational wave packets have been studied in several diatomic molecules, including the alkali dimers ($Li_2, Na_2, ..., Cs_2$),[1–10] NaI,[11] and I_2.[12,13] Since the production of a wave packet entails the coherent excitation of two or more states, generating a vibrational wave packet with a single optical pulse requires that the bandwidth of that pulse exceed the local vibrational state separation ($\approx\omega_e-2v\,\omega_e x_e$) for the electronic state under study. Experiments to date have been confined to diatomics for which the vibrational frequency $\omega_e<200\,cm^{-1}$ and have generally involved detecting wave packet motion by combining photoionization of the molecule with time-of-flight photoelectron energy or ion mass spectrometry analysis.

Recently, vibrational wave packets in the $C\,^1\Pi_u$ state of Cs_2 were produced and examined by laser pump–probe spectroscopy experiments in which the temporal history of the wave packet was recorded by monitoring the time and energy-integrated photoelectron current.[3,4] Because of the large difference between the equilibrium internuclear separations for the $Cs_2(C)$ state and the ground state of the dimer ion ($R_e\{Cs_2^+(X)\}-R_{eC}\approx0.75$ Å), the $C\,^1\Pi_u$ state is photoionized in a narrow Franck–Condon region located near the classical inner turning points for the $Cs_2^+(X,v'\approx65-90)$ vibrational levels. Consequently, wave packets in the $Cs_2(C\,^1\Pi_u)$ state give rise to a photoelectron current that is deeply modulated as the time delay (Δt) between the pump and probe pulses is varied. Since this approach to wave packet detection does not rely on resolving electron or ion energies, the photoelectron signal is expected[14] to exhibit significant modulation *only* if the potential surfaces of the intermediate and final (ion) molecular states differ appreciably.

In this paper, similar experiments are reported for the $B\,^1\Pi_u$ and $D\,^1\Sigma_u^+$ states of Cs_2. Two color pump–probe experiments for the $B\,^1\Pi_u$ state entailed exciting the molecule in the ~740–790 nm region and photoionizing the B state at wavelengths between 565 nm and 600 nm. For the $D\,^1\Sigma_u^+$ experiments, the pump wavelength was varied over a ~35 nm interval (575–610 nm) whereas the central probe wavelength was fixed at 750 nm. Comparison of the experimental data with wave packet transients calculated from the density matrix formalism[15] yields improved values for the equilibrium internuclear separation for the $B\,^1\Pi_u$ state and T_e for the Cs_2^+ ion ground state.

The B and D states of Cs_2 are interesting for wave packet experiments for several reasons. In contrast to $Cs_2(C\,^1\Pi_u)$, for example, the value of R_e for the $B\,^1\Pi_u$ state differs from that for $Cs_2^+(X)$ by <0.4 Å.[4,16,17] Thus, the B state provides an interesting test of the extent of applicability of the photoelectron current wave packet detection technique. The $D\,^1\Sigma_u^+$ state was first characterized comparatively recently (1982),[18,19] is known to have an equilibrium internuclear separation intermediate to those for the ground states of the dimer and dimer ion, and $R_{eD}-R_{eX}\simeq1$ Å. Consequently, producing and detecting D state wave packets is complicated by small $D-X$ Franck–Condon factors (FCFs). Furthermore, photoexcitation of $D\,^1\Sigma_u^+$ from ground at ~580–600 nm populates the $v'\approx40-50$ vibrational states that are known from high resolution laser spectroscopic experiments[20–23] to be strongly perturbed by the bound $2\,^3\Pi_{ou}$ state. Blanchet

[a]Present address: Oration, LLC, 7 West 41st Ave., Suite 78, San Mateo, CA 94403.

et al.[5,6] have recently reported producing wave packets in the $Cs_2(B)$ state in single color pump–probe experiments at 768 nm. Because of the pump wavelength and cooling of the dimers in a supersonic expansion, the $B(v'=0,1)$ states were the dominant contributors to the wave packet composition. The experiments described here involve a Cs_2 ground state population that is thermalized at 260–300 °C, which results in wave packets on the intermediate potential surface ($B\,^1\Pi_u$ or $D\,^1\Sigma_u^+$) comprising at least 15–20 vibrational states. Although such wave packets dephase more quickly than do their counterparts consisting of only a few vibrational levels, combining the density matrix formalism with data acquired by varying experimental parameters (the pump and probe wavelengths, in particular) allows one to isolate key spectroscopic constants of the intermediate and final electronic states.

II. EXPERIMENT

The experimental arrangement and data acquisition techniques are similar to those described in detail previously[3,4] and will only be reviewed here. Briefly, pulses having temporal widths ($sech^2$) of 80–100 fs and energies of ~300 μJ are produced at 30 Hz by a colliding pulse mode-locked (CPM) oscillator and a four stage dye amplifier system driven by a frequency-doubled Nd:YAG laser. Supercontinua are produced by focusing the pulses into water and, after dividing each pulse into two with a beamsplitter, one is time-delayed with respect to the other by a retroreflector mounted onto a computer-controlled translation stage. Interference filters remove ~10 nm (FWHM) spectral segments from each pulse and both are focused into a heatpipe containing Cs vapor at pressures ranging from 10 to 100 Torr ($1.5\times10^{17}\lesssim[Cs]\lesssim1.2\times10^{18}\,cm^{-3}$). A cylindrical diode (proportional counter) installed in the heatpipe allows for the time and energy-integrated photoelectron current to be measured. Care must be taken to ensure that the proportional counter is not saturated.

III. RESULTS AND DISCUSSION

A. Temporal domain data

Experiments were carried out for several values of the central pump wavelength (λ_1) while the probe wavelength (λ_2) and Cs number density in the heat pipe were held constant. Representative results for vibrational wave packets produced in the $Cs_2(B\,^1\Pi_u)$ state are presented in Fig. 1 which shows the variation of the total photoelectron current with Δt. Three traces obtained for $\lambda_1=758$ nm and $\lambda_2=600$ nm are shown to illustrate the reproducibility of the experiments. The periodicity of the oscillations in the photoelectron signal (~1 ps) is in agreement with the B state classical vibrational period, $(c\omega_e)^{-1}\cong0.97$ ps [where the vibrational frequency for the B state, ω_e, is 34.3 cm^{-1} (Refs. 16, 24)], as well as the results of Ref. 6. Figure 2 presents data representative of that acquired for nine values of λ_1 between 751 and 771 nm, with λ_2 again fixed at 600 nm. Notice that dephasing of the vibrational wave packet occurs within $\Delta t\approx6$ ps and photoionization traces having the highest S/N ratios and largest modulation depths were obtained for 751

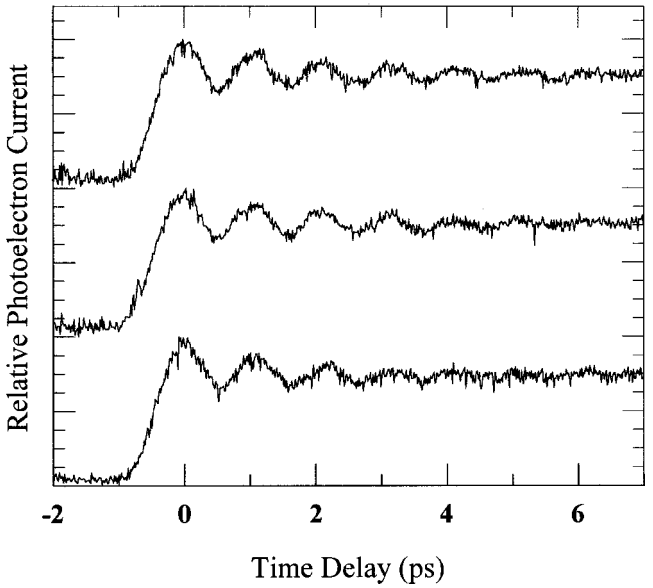

FIG. 1. Dependence of the photoionization current on the time delay (Δt) for vibrational wave packets in the $B\,^1\Pi_u$ state. Three scans, each obtained for $\lambda_1=758$ nm and $\lambda_2=600$ nm, are shown to illustrate the reproducibility of the experiment and the baselines for the traces have been intentionally offset for clarity. The heatpipe temperature was fixed at 573 K.

$\lesssim\lambda_1\lesssim763$ nm. For pump wavelengths (λ_1) beyond ~765 nm, signal quality degraded and wave packet dephasing accelerated. This is to be expected for two reasons. As a result of the $B-X$ FCFs[16] and the concomitant $B\leftarrow X$ absorption spectrum (cf. Fig. 3), a substantial fraction of the B state population produced by the pump pulse resides in $v'\geqslant20$ states. As an example, Fig. 4 illustrates the vibrational distribution of the $Cs_2(B)$ and $Cs_2^+(X)$ populations for T

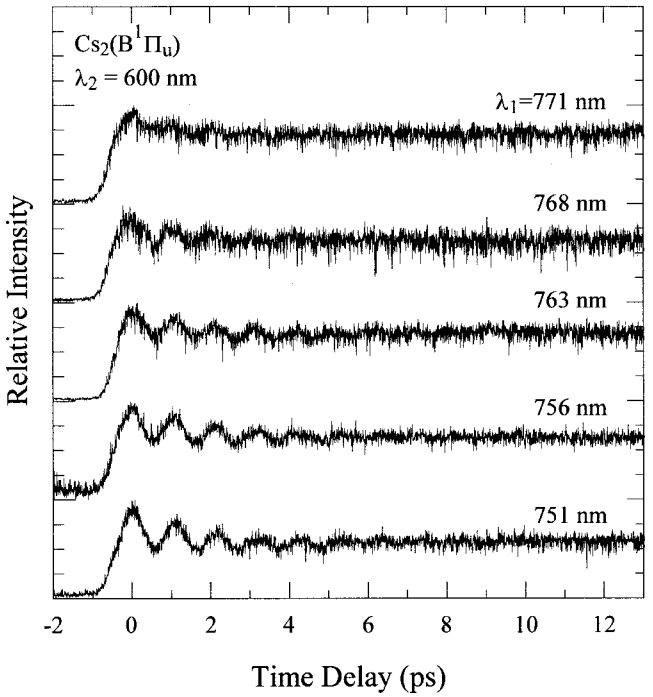

FIG. 2. Comparison of the $B\,^1\Pi_u$ photoionization traces acquired for several values of the central wavelength λ_1 with λ_2 fixed at 600 nm. The heatpipe temperature for each data set is either 533 K or 573 K.

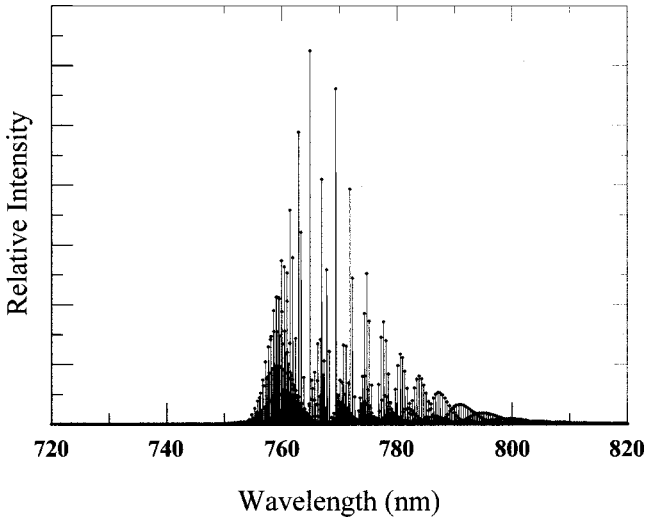

FIG. 3. Stick absorption spectrum calculated for the $B \leftarrow X$ transition of Cs_2 from the Franck–Condon factors (FCFs) of Ref. 16 and assuming a temperature of 600 K. The envelope is in agreement with experiment.

$=573\,\mathrm{K}$, calculated from the Cs_2 (X and B) and $Cs_2^+(X)$ spectroscopic constants to be discussed in Sec. III B 1, and the measured pump and probe spectra. Second, the anharmonic constant $\omega_e x_e$ for the $B\,^1\Pi_u$ state is $\sim 0.08\ \mathrm{cm}^{-1}$ (cf. Dunham coefficients of Ref. 16) which is roughly a factor of 2 larger than that for the $C\,^1\Pi_u$ state ($\omega_e x_e = 0.042\ \mathrm{cm}^{-1}$).[18] Since wave packet dephasing is dependent on both the anharmonic constant for the state under study and the number of vibrational levels in the excited state ensemble from which the wave packets are produced, one would expect the greater anharmonicity of the $B\,^1\Pi_u$ state to lead to faster dephasing of the wave packet. This is consistent with our observation of B state wave packet dephasing in ~ 6 ps, in contrast to wave packets produced in the C state which have been shown[3,4] to dephase in 10–15 ps.

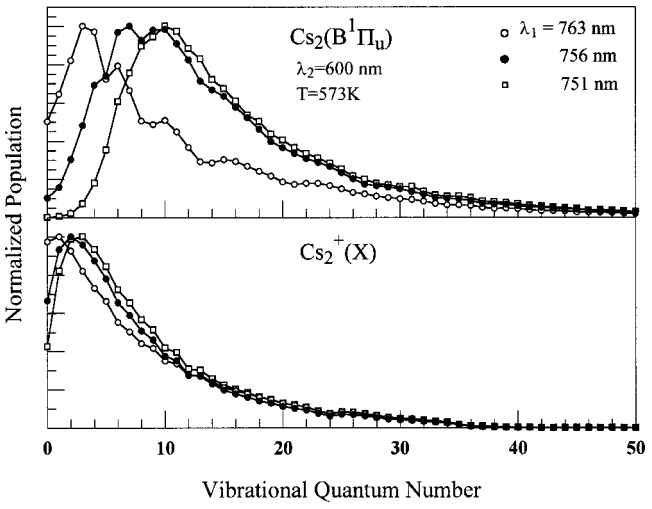

FIG. 4. $Cs_2(B)$ and $Cs_2^+(X)$ vibrational population distributions for a temperature of 573 K, calculated for three values of the central pump wavelength (λ_1) and λ_2 set at 600 nm. Also, the calculations adopted the $Cs_2(B,X)$ spectroscopic data of Ref. 16 and the Cs_2^+ ground state constants given in Sec. III B 1.

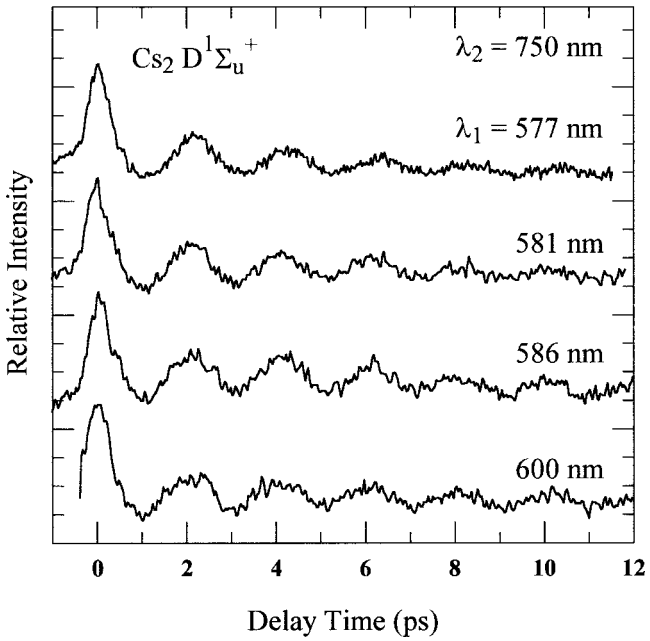

FIG. 5. Scans of photoelectron current as a function of Δt for vibrational wave packets in the $Cs_2(D\,^1\Sigma_u^+)$ state. The probe wavelength is fixed at 750 nm and data for central pump wavelengths (λ_1) between 577 and 600 nm are shown.

The data of Figs. 1 and 2 differ from those of Refs. 5 and 6 in two respects. Because the wave packets in the experiments of Blanchet and co-workers were composed primarily of the $B(v'=0,1)$ vibrational wave functions (due to cooling of Cs_2 in a supersonic expansion and the B–X FCFs), they dephased slowly and oscillations in the Cs_2^+ ion signal owing to motion of the B state wave packet persist for tens of ps. In the present experiments, significant contributions from more than 20 B state vibrational levels result in much quicker dephasing of the wave packet, although excited state vibrational levels higher than those accessed in Refs. 5 and 6 are populated and probed. Also, the tunability of the pump (λ_1) and photoionization (λ_2) pulses permits one to observe the wavelength dependence of the temporal and spectral characteristics of the wave packet transients, in addition to optimizing the $Cs_2(B,v')$ ionization probability. Previous experiments[4] examining the $C\,^1\Pi_u$ state of Cs_2 have shown the latter to be a key factor in determining the detectability of the wave packet.

Photoionization data similar to those of Fig. 2 but for rovibrational wave packets generated in the $D\,^1\Sigma_u^+$ state of Cs_2 are illustrated in Fig. 5. For these experiments, the central probe wavelength (λ_2) was fixed at 750 nm (with a 25 nm FWHM bandpass filter) while λ_1 was varied over the 575–610 nm region. For $\Delta t < 0$, no signal is generally detected (as one expects since the probe precedes the pump), except when the pump wavelength is also suitable for photoionizing the B state. In such a case ($\lambda_1 = 600\,\mathrm{nm}$, $\lambda_2 = 750\,\mathrm{nm}$, for example, cf. Fig. 2), B state wave packets are observed for $\Delta t < 0$ and D state wave packets when $\Delta t > 0$. Because of the FCFs for the $D \leftarrow X$ transition of Cs_2 (to be addressed in Sec. III C), $D \leftarrow X$ absorption is approximately two orders of magnitude weaker than that for the $C \leftarrow X$ transition. Note that the periodicity of the signals in Fig. 5 is ≈ 2

ps which implies an *average*, local vibrational state energy spacing in the $D\,^1\Sigma_u^+$ state of $16.7\,\mathrm{cm}^{-1} < \omega_{eD}$ ($\sim$19.3 cm^{-1}—Refs. 20–23), corresponding to ΔG in the vicinity of $v'=36$. However, as will be discussed later, the $D-X$ FCFs favor transitions to $D(v'\approx 40-50)$, vibrational levels whose positions have been shown to be perturbed through the interaction of $D\,^1\Sigma_u^+$ with the bound $2\,^3\Pi_{ou}$ state. The latter is correlated, in the separated atom limit, with $\mathrm{Cs}(5d\,^2D_{3/2}) + \mathrm{Cs}(6s\,^2S_{1/2})$ (Refs. 22, 23, 25) and shifts the $35 \leqslant v' \leqslant 58$ states by as much as 0.7 cm^{-1} (Ref. 22). From rotational linewidth measurements, Katô *et al.*[22] inferred the predissociation rates for the $D\,^1\Sigma_u^+(v'=46, J'=30-70)$ states to be $10^9\,\mathrm{s}^{-1}$. In light of these comments, it is interesting to note that dephasing of the wave packets in Fig. 5 occurs more slowly ($\sim$7–9 ps) than is observed for the B state experiments, a result that is partially attributable to the fact that $\omega_e x_e(D) < \omega_e x_e(B)$. The irregularity of the D state rovibrational spacing in this region might otherwise be expected to lead to more rapid dephasing of the wave packet than that characteristic of the B state.

B. Analysis of $B\,^1\Pi_u$ wave packets

1. Density matrix theory

Numerical calculations of the temporal behavior of vibrational wave packets in the B (and D) states have been carried out according to the density matrix approach described in Ref. 15 and applied in Ref. 4 to the $\mathrm{Cs}_2(C\,^1\Pi_u)$ state. The potential adopted for the $X\,^1\Sigma_g^+$ state was generated by the IPA (inverted perturbation approach)[26] based on the eigenenergies, measured by Weickenmeier *et al.*,[27] for the lowest 138 vibrational levels. The $B\,^1\Pi_u$ vibrational eigenenergies, which have been measured up to $v'=20$ by Doppler-free polarization spectroscopy,[16] were extrapolated to $v'=50$ by a polynomial (Dunham-type) expansion, where $G(v'=50)=1520\,\mathrm{cm}^{-1}$, which is still well below the B state dissociation energy ($\sim$2338 cm^{-1}).[16] The $B\,^1\Pi_u$ potential was then constructed by the IPA.

Turning now to the final state for the wave packet production and detection sequence $[\mathrm{Cs}_2^+(X\,^2\Sigma_g^+)]$, a source of uncertainty in the calculations is the absence in the literature of measured spectroscopic constants for the dimer ion ground state.[4] Pseudopotential and effective core potential calculations for $\mathrm{Cs}_2^+(X)$ predict $R_e(X)=5.25\pm0.05$ Å and $\omega_e=34\pm3\ \mathrm{cm}^{-1}$ (Refs. 17, 28–30) but recent simulations by Braun *et al.*[31] of the $C\,^1\Pi_u$ wave packet experiments of Ref. 3 suggest revising $R_e[\mathrm{Cs}_2^+(X)]$ down by 6% to 4.97 Å. Since the $\mathrm{Cs}_2^+(X\,^2\Sigma_g^+)$ state is not well-characterized, in all of the calculations to follow its potential is approximated by a Morse potential for which the larger value for R_e (5.25 Å) was adopted and the vibrational frequency was taken to be 34 cm^{-1}. On the basis of several theoretical values[28–30] and an experimental lower limit,[32] D_e for the dimer ion ground state is initially taken to be $5060\pm800\,\mathrm{cm}^{-1}$, which yields $T_e[\mathrm{Cs}_2^+(X)]=30\,000\pm800\,\mathrm{cm}^{-1}$ if the dissociation energy for the neutral dimer ground state ($X\,^1\Sigma_g^+$) is assumed to be $D_e=3649.5\,\mathrm{cm}^{-1}$.[27] It is not expected that the description of the $\mathrm{Cs}_2^+(X)$ state by a Morse potential introduces significant error into the calculations because the FCFs for the ionization of the $B\,^1\Pi_u$ state $[\mathrm{Cs}_2^+(X) \leftarrow \mathrm{Cs}_2(B)]$ strongly favor transitions terminating on the lowest vibrational levels of the $X\,^2\Sigma_g^+$ state (cf. Fig. 4).

Rotationless wave functions for the Cs_2 X and B states as well as the ground state of Cs_2^+ were calculated by the Numerov method. FCFs for the $\mathrm{Cs}_2(B \leftarrow X)$ and $\mathrm{Cs}_2^+(X) \leftarrow \mathrm{Cs}_2(B)$ transitions were then computed. From the measured pump and probe laser spectra, the calculated FCFs, and an assumed Boltzmann distribution for the Cs_2 ground state population, the experimentally determined photoelectron current-time delay (Δt) scans were simulated by the density matrix technique proposed by Gruebele and Zewail.[15] Since the ionization signal reflects the probability of finding a molecule in the final $[\mathrm{Cs}_2^+(X)]$ state for a given value of Δt, the wave packet transient can be expressed as the sum of vibrational and rotational terms:

$$
\begin{aligned}
I(\Delta t) \propto & \left[\sum_{v_1', v_2' < v_1'} \frac{2}{1+b_{12}^2(\Delta t)^2} \left[\cos(2\pi c \Delta t \cdot \Delta G_{12}) + b_{12} \Delta t \sin(2\pi c \Delta t \cdot \Delta G_{12}) \right] \right. \\
& \left. + \frac{1}{2} \sum_{v_1', v_2'} (1 - b_{\mathrm{rot}}^2 (\Delta t)^2) \cos(2\pi c \Delta t \cdot \Delta G_{12}) e^{-b_{\mathrm{rot}}^2 (\Delta t)^2} \right] \\
& \times \sum_{v''} F(v'', v_1') F(v'', v_2') E_P(\omega_{v''} - \omega_{v_1'}) E_P(\omega_{v''} - \omega_{v_2'}) \sum_{v} F(v_1', v) F(v_2', v) E_L(\omega_{v_1'} - \omega_v) E_L(\omega_{v_2'} - \omega_v) e^{-E_v/kT}, \qquad (1)
\end{aligned}
$$

where

$$
b_{12} = \frac{2\pi \alpha_e' kT}{B_e' h} (v_1' - v_2'), \qquad (2)
$$

$$
b_{\mathrm{rot}} = 4\pi B_e' \sqrt{\frac{ckT}{B_e h}}, \qquad (3)
$$

v, v', and v'' represent Cs_2 ground ($X\,^1\Sigma_g^+$), intermediate ($B\,^1\Pi_u$ or $D\,^1\Sigma_g^+$), and ion $[\mathrm{Cs}_2^+(X)]$ vibrational states, respectively, B_e is the $X\,^1\Sigma_g^+$ rotational constant, while B_e' and α_e' are rotational constants for the intermediate state,[16,22,23] $F(v_a, v_b)$ is the FCF associated with the transition between the indicated vibrational and electronic states, $E_L(\omega)$ and

$E_P(\omega)$ are the pump and probe laser spectra, respectively, $\Delta G_{12} \equiv E(v_1', J'=0) - E(v_2', J'=0)$ is the difference in the energies of the two intermediate state vibrational levels v_1' and v_2', and E_v (which appears in the Boltzmann term) is the energy of the $X\,^1\Sigma_g^+$ $(v, J=0)$ level. Although Eq. (1) does not explicitly sum over all J, it is valid for the experiments reported here because the ground state rotational temperature ($\approx$vapor temperature) allows for the sum over J to be approximated as an integral.[15] One simplification, however, that was *not* made[15] in these calculations was to restrict $v_1' - v_2'$ to be solely ± 1. The bandwidth of the amplified CPM laser pulses compels us to consider higher order coherences (± 2, ± 3,...).

The vibrational transient, described by the first two terms of Eq. (1), is expressed in terms of a sinusoid of frequency ω_e' and a rotational dephasing time, b_{12}^{-1}, which is $\approx$21 ps (considering only $\Delta v' = \pm 1$ coherences) for the $B\,^1\Pi_u$ state of Cs_2. For the B state experiments reported here, however, a key factor in determining the wave packet dephasing time is the anharmonic coefficient $\omega_e' x_e'$ which causes dephasing on the time scale of $t_d \approx (4\omega_e' x_e' \cdot n \cdot c)^{-1}$, where n is the number of $B\,^1\Pi_u$ state vibrational levels composing the wave packet. For $n=15$ (cf. Fig. 4), $t_d \cong 7$ ps which is consistent with experimental observations.

The term in Eq. (1) involving $b_{\rm rot}$ constitutes the rotational transient that dephases on a time scale of $b_{\rm rot}^{-1} \cong 1.4$ ps. Because of its small magnitude, the rotational transient has the primary effect of increasing the amplitude of the first two oscillations in the photoelectron current versus Δt data scans (Figs. 1, 2, and 5).

For experimental situations in which the laser chirp cannot be neglected (i.e., the change in phase over the laser bandwidth is $\geqslant \pi$), it can be explicitly incorporated into Eq. (1) by adding

$$\Delta\theta \equiv \theta(v, v_1') - \theta(v, v_2') + \theta(v_1', v'') - \theta(v_2', v'') \qquad (4)$$

to the argument of each sinusoidal function, where $\theta(v_a, v_b)$ is the spectral phase of the pump or probe laser pulse at the frequency corresponding to the energy difference between v_a and v_b. When the chirp is linear, for example, this phase factor will be proportional to $((\omega_{v_b} - \omega_{v_a}) - \omega_0)^2$, where ω_0 is the center frequency of the laser pulse. Unfortunately, accounting for chirp in the calculations complicates the separation of the four-dimensional sum over v, v_1', v_2', and v'' into sets of lower-order sums as indicated in Eq. (1). The result is a drastic increase in computational time.

2. Comparison of theory with experiment

Simulating the experimentally observed $B\,^1\Pi_u$ vibrational transients with the density matrix formalism offers the opportunity to isolate particular Cs_2 spectroscopic constants. In particular, optimizing the fit between simulations and experimental data with respect to specific temporal and spectral characteristics of the transient allows for the values for the B state equilibrium internuclear separation (R_e) and T_e for the Cs_2^+ ground state to be improved.

One characteristic or observable of the Cs_2 (B and D) wave packet transient that serves as a test of the theoretical predictions is the transient's modulation depth. Somewhat arbitrarily defined as the difference between the magnitude of the photoelectron current peak at $\Delta t = 0$ and the first local minimum in the signal, the modulation depth is a rapidly varying function of the central pump wavelength λ_1. An examination of Fig. 2 suggests, and the open circles (○) of Fig. 6 confirm, that the modulation depth of the $Cs_2(B\,^1\Pi_u)$ transients peaks for $\lambda_1 \sim 751$ nm when the probe wavelength (λ_2) is fixed at 600 nm. In contrast, numerical simulations of the vibrational-rotational transient, based on the density matrix model and spectroscopic constants of Sec. III B 1, show quite different behavior, predicting that the maximum modulation depth of the transients will be observed at longer wavelengths ($\lambda_1 \cong 760$ nm).

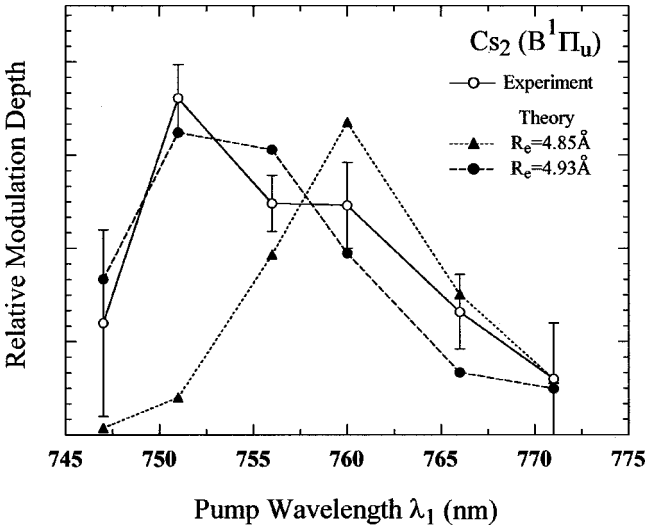

FIG. 6. Dependence of the experimentally observed and calculated $Cs_2(B\,^1\Pi_u)$ wave packet modulation depth on the pump wavelength λ_1: (○) measured values for $T = 533$ K and λ_2 fixed at 600 nm; (▲) values calculated from the density matrix model and spectroscopic constants described in Sec. III B 1, including $R_e(B\,^1\Pi_u) = 4.85$ Å; (●) theoretical results for $R_e(B) = 4.93$ Å (all other spectroscopic constants unchanged). The estimated uncertainty ($\pm 1\ \sigma$) in each experimental measurement is also shown.

As one might expect, the calculated modulation depth is found to be relatively insensitive to the Cs_2^+ spectroscopic constants. Varying the $Cs_2^+(X)$ spectroscopic constants ω_e and R_e by more than one standard deviation (σ) results in only a negligible change in the value of χ^2 describing the fit of the theoretical transient to the experimental data. Specifically, $\Delta\chi^2 \leqslant 3\%$ per $\pm\sigma$. Furthermore, a sensitivity analysis with respect to $T_e[Cs_2^+(X)]$ shows the assumed value ($3 \times 10^4\ cm^{-1}$) to actually yield the *best* fit (i.e., minimum χ^2) between theory and experiment.

All of the remaining constants required by the calculations have been measured, directly or indirectly, by laser spectroscopy, and the ground state constants (Dunham coefficients) have been determined to high precision. Despite the excellent experiments by Diemer *et al.*,[16] however, the $B\,^1\Pi_u$ constants are not known to the same degree of precision. The equilibrium internuclear separation (R_e), for example, was determined in Ref. 16 by constructing the $B\,^1\Pi_u$ potential from the Dunham coefficients by the RKR and IPA methods and, subsequently, calculating the rotational con-

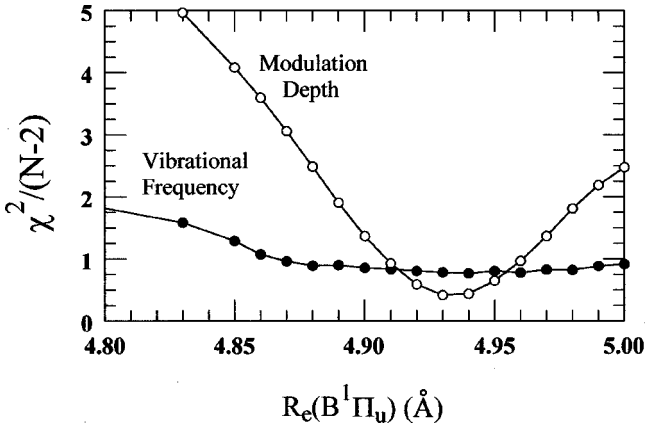

FIG. 7. (○): Variation of χ^2/N-2 (describing the difference between the modulation depths of experimental transients for $747 \leqslant \lambda_1 \leqslant 771$ nm and their theoretical counterparts) with the assumed values of R_e for the $Cs_2(B\,^1\Pi_u)$ state. For these data, N (the number of values of λ_1 for which experiments and simulations were conducted) is six. (●): Dependence of χ^2/N-2 on R_e when the predicted vibrational frequency of the simulated transients is compared with that for the experimentally measured wave packet transient. For both curves shown, $\chi^2 < 1$ for $4.91 \leqslant R_e(B) \leqslant 4.96$ Å.

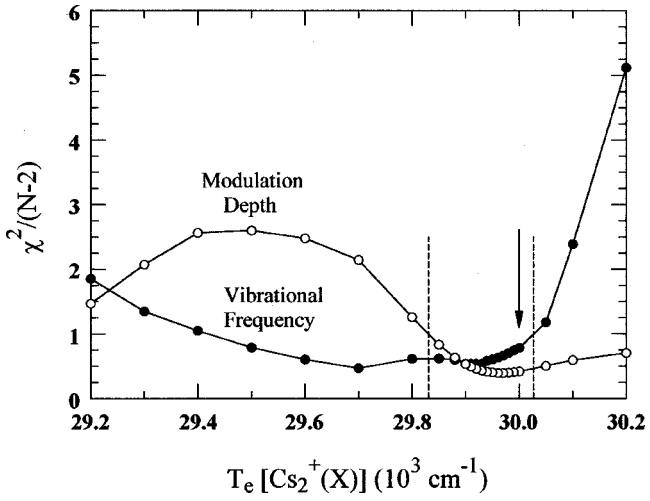

FIG. 8. Data similar to those of Fig. 7 but χ^2 for two separate observables is now illustrated as a function of T_e for the Cs_2^+ ground state. Together the two curves indicate that T_e lies between ~29 830 and 30 030 cm^{-1}. The vertical arrow indicates the value for T_e (30 000 cm^{-1}) originally adopted in the wave packet simulation model (cf. Sec. III B 1). For details regarding the experimental conditions associated with the data for each curve, please refer to the text.

stants B_v from the vibrational wave functions for the state. In this way, R_e was estimated to be 4.85 Å. Utilizing a relativistic effective core potential, Jeung *et al.*[33] calculated $R_e(B)$ to be 4.86 Å.

Simulations show that the quality of the fit between the theoretical and experimental B state transients is quite sensitive to the assumed value of R_e. Consider, for example, Fig. 7. Vibrational transients were calculated for 17 values of $R_e(B)$ ranging from 4.83 Å to 5.0 Å and six values of λ_1 ($747 \leqslant \lambda_1 \leqslant 771$ nm, with λ_2 held constant at 600 nm). For a given value of R_e, the modulation depth associated with each theoretical transient was compared with the experimental result and χ^2 was then calculated by summing the squares of the differences between theory and experiment over all six λ_1 studied for that value of R_e. That is, $\chi^2 = \Sigma_i \{d_{i_{\rm exp}} - d_{i_{\rm theory}}\}^2 \sigma_{i_{\rm exp}}^{-2}$, where d represents the modulation depth for a specific transient. As illustrated by the open circles of Fig. 7, increasing R_e from 4.85 Å results in a rapid drop in χ^2 and $\chi^2/(N-2)$ [where N=6] <1 for $4.91 \leqslant R_e(B) \leqslant 4.96$ Å. An uncertainty for the value of R_e presented in Ref. 16 was not given and, on the basis of extensive comparisons of experiment with theory, it is proposed here that a more precise value for the $B\,^1\Pi_u$ equilibrium internuclear separation is 4.93 ± 0.03 Å. Returning now to Fig. 6, the solid dots depict the dependence of the calculated modulation depth on λ_1 if $R_e = 4.93$ Å. As a check on this revised value, the variation of χ^2 with changes in the $Cs_2^+(X)$ constants was revisited, now assuming $R_e(B\,^1\Pi_u)$ to be 4.93 Å. As before, the fluctuations in χ^2 were found to be negligible for variations exceeding $\pm\sigma$ in either ω_e or R_e. A key result of this work, then, is that ultrafast experiments conducted in the temporal domain are able, by varying the pump and probe spectra and computational analysis of the resulting rovibrational transients, to determine molecular spectroscopic constants or, potentially, improve upon those measured in the frequency domain.

Further confirmation for the increase in $R_e(B)$ proposed above is provided by an examination of the frequency composition of the experimental and calculated wave packet transients. Fourier transform (or Maximum Entropy Method, MEM)[15] frequency spectra of the experimental data of Fig. 2, for example, show a dominant peak at $31.4 \pm 0.8\ cm^{-1}$ for $\lambda_1 = 751$ nm and $\lambda_2 = 600$ nm, where the uncertainty represents one standard deviation. When λ_1 is increased to 768 nm (with λ_2 held fixed at 600 nm), the peak response in the frequency spectrum shifts to 33.8 cm^{-1}. These results are to be expected because $\omega_e(B\,^1\Pi_u) = 34.3\ cm^{-1}$ (Ref. 16) and 31.4 cm^{-1} corresponds to the ΔG value for the B state in the vicinity of $v' = 18$, which is approximately $\langle v' \rangle (\cong 16)$ for the $B\,^1\Pi_u$ population distribution produced by the pump ($\lambda_1 = 751$ nm, cf. Fig. 4). As λ_1 is increased, however, the $B-X$ FCFs favor excitation of lower-lying B state vibrational levels ($\langle v' \rangle \cong 14$ and 12 for $\lambda_1 = 756$ and 763 nm, respectively) and, hence, the ΔG value reflected in the wave packet motion rises.

In an effort to evaluate from a different perspective the value of $R_e(B\,^1\Pi_u)$ presented earlier, the frequency spectra of 20 wave packet transients, acquired experimentally for various values of λ_1, λ_2 and temperature, were calculated. For each transient, the experimentally determined fundamental frequency was compared with that resulting from the simulations and the results are displayed in Fig. 7 by the solid circles. In this case, χ^2 for the observable (wave packet fundamental frequency) exhibits a broad minimum in R_e and falls below one for $R_e \gtrsim 4.86$ Å. This result provides further support for the conclusion that $R_e(B\,^1\Pi_u)$ is slightly larger than the value estimated in Ref. 16.

A similar process was then used to re-evaluate the Cs_2^+ ground state constants. Taking $R_e(B)$ now to be 4.93 Å, the Cs_2^+ spectroscopic constants (ω_e, R_e, and T_e) were altered from the values of Sec. III B 1 and, as shown in Fig. 8, the most striking results were obtained for T_e. The experimental data from which these results were calculated were those described earlier in connection with the study of the modu-

lation depth (six sets: various λ_1, $\lambda_2 = 600$ nm, $T = 533$ K) and vibrational frequency (20 sets: various λ_1, λ_2, and T) of the transients. Two curves are given in Fig. 8, both of which illustrate the dependence of χ^2 on the assumed value of T_e for the Cs_2^+ ground state. The open circles represent $\chi^2/(N-2)$ associated with the modulation depths of the simulated and experimental wavepacket transients. As noted earlier, χ^2 for this particular observable takes on its minimum value in the vicinity of the value of $T_e(30\,000\ \mathrm{cm}^{-1})$ adopted originally in the model and denoted by the vertical arrow. For $29\,900 \lesssim T_e \lesssim 30\,100\ \mathrm{cm}^{-1}$, χ^2 is essentially flat but increases rapidly for values of T_e below $\sim 29\,850\ \mathrm{cm}^{-1}$. In particular, χ^2 rises above one for $T_e \lesssim 29\,830\ \mathrm{cm}^{-1}$ (indicated by the left dashed vertical line in Fig. 8). When monitoring the (fundamental) vibrational frequency of the wavepacket data (denoted in Fig. 8 by the solid dots), however, χ^2 changes relatively slowly until T_e is increased beyond $30\,000\ \mathrm{cm}^{-1}$. At $\sim 30\,300\ \mathrm{cm}^{-1}$ (indicated by the second dashed vertical line, at right), χ^2 surpasses one and rises rapidly. On the basis of these results, we propose the revised value of $29\,930 \pm 100\ \mathrm{cm}^{-1}$ for T_e of $Cs_2^+(X\,^2\Sigma_g^+)$, for which the lower limit of the constant is defined by the modulation depth data of Fig. 8 while the upper limit is set by the comparison between the vibrational frequencies of the experimental and theoretical wavepacket data. Revising T_e also implies that $D_e[Cs_2^+(X)]$ is now $5130 \pm 100\ \mathrm{cm}^{-1}$ which is in agreement with the lower limit of 0.59 ± 0.06 eV established by Helm and Möller[32] from photodissociation experiments.

This suggested value for T_e is only slightly smaller than the value originally adopted for the computer model but the comparison between simulation and experiment has permitted the estimated uncertainty in the constant to be reduced considerably. However, it should also be mentioned that $T_e[Cs_2^+(X)] = 29\,930\ \mathrm{cm}^{-1}$ as proposed here is considerably larger than calculations would suggest ($29\,200$–$29\,400\ \mathrm{cm}^{-1}$).[28–30] Finally, analyses similar to that of Fig. 8 for ω_e and R_e of the Cs_2^+ ground state yield weak variations in χ^2 (i.e., $\Delta\chi^2$ changes by $< \pm 10\%$ per σ) when either constant is altered from its assumed value ($\omega_e = 34\ \mathrm{cm}^{-1}$ and $R_e = 5.25$ Å).

Before leaving this section, the potential contribution of higher-order coherences (interactions between nonadjacent vibrational levels) and laser chirp to B state wave packet data (e.g., Figs. 1 and 2) should be considered. Figures 9 and 10 show the results of simulating wave packet transients produced by pump wavelengths of 751 nm and 762 nm and $\lambda_2 = 600$ and 580 nm, respectively. For both experimental scans (photocurrent as a function of Δt), three simulations are given. The first [part (b)] of Figs. 9 and 10 includes both $\Delta v = \pm 1$ coherences and the chirp of the pump and probe pulses. Specifically, based on spectral and cross-correlation measurements, a linear positive chirp, corresponding to the broadening of nearly transform-limited pump and probe pulses to ~ 180 fs at the heatpipe, was incorporated into the simulations. Doing so improves the fit of all of the calculated transients to the data. If higher-order ($|\Delta v| > 1$) coherences are now also incorporated into the calculations, trace (c) results. The beneficial impact of accounting for the known laser pulse chirp is clear from panel (d) of Fig. 9 which illustrates the transient calculated when $|\Delta v| \geqslant 1$ coherences are incorporated into the calculations but chirp is neglected. A similar comparison between experiment and simulations is presented in Fig. 10 for $\lambda_1 = 762$ nm and $\lambda_2 = 580$ nm. MEM frequency spectra of the eight wave packet transients of Figs. 9 and 10 are shown in Fig. 11. Comparing the three figures, it is obvious that higher-order coherences manifest themselves in the frequency domain as harmonics of the fundamental vibrational frequency. In the temporal domain, however, the $|\Delta v| > 1$ coherences have the effect of narrowing the peaks in the transients [cf. panel (d) of Figs. 9 and 10], a result that is at odds with experiment. Accounting for the chirp of the pump and probe laser pulses ameliorates both of these effects. For all of the data obtained to date, the amplitude of the $\Delta v' = 2$ peak in the frequency domain, for example, is consistently $\leqslant 5\%$ of that for the fundamental. As illustrated in parts (d) and (h) of Fig. 11, the simulations are unable to account for this fact if the chirp of the laser pulse is ignored. If, however, the linear chirp is now imposed onto the pump and probe pulses, the amplitudes of the second

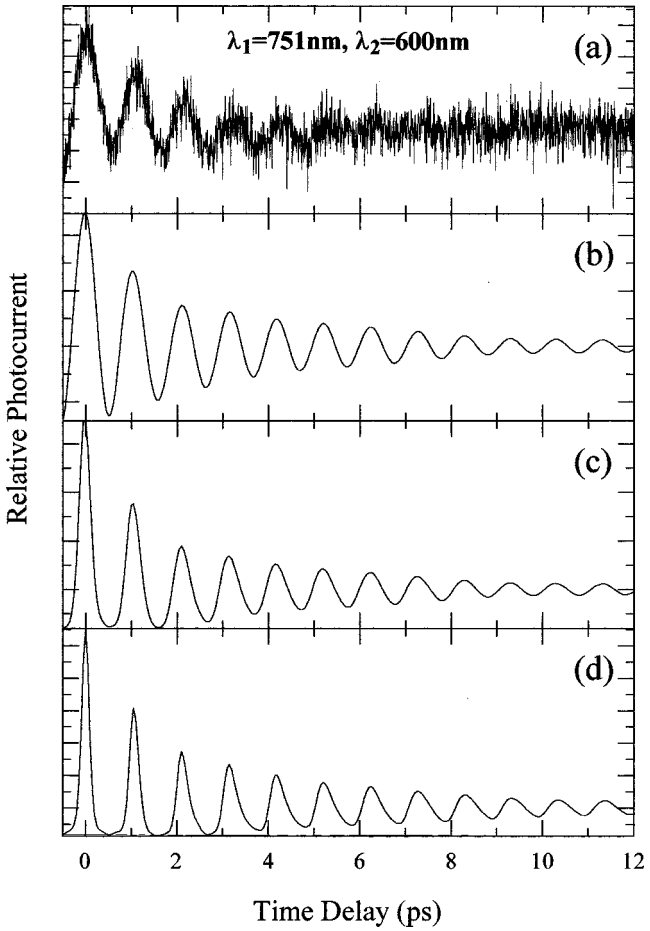

FIG. 9. Comparison of experimental and calculated $Cs_2(B\,^1\Pi_u)$ wave packet data for $\lambda_1 = 751$ nm and $\lambda_2 = 600$ nm: (a) experimental scan of photocurrent vs Δt; (b) simulation of the data in which only $\Delta v = \pm 1$ coherences are considered, along with pump and probe pulse chirp; (c) simulation including both higher order coherences ($|\Delta v| > 1$) and laser chirp; (d) incorporating higher-order coherences but not laser chirp. Again, the traces have been intentionally offset for clarity.

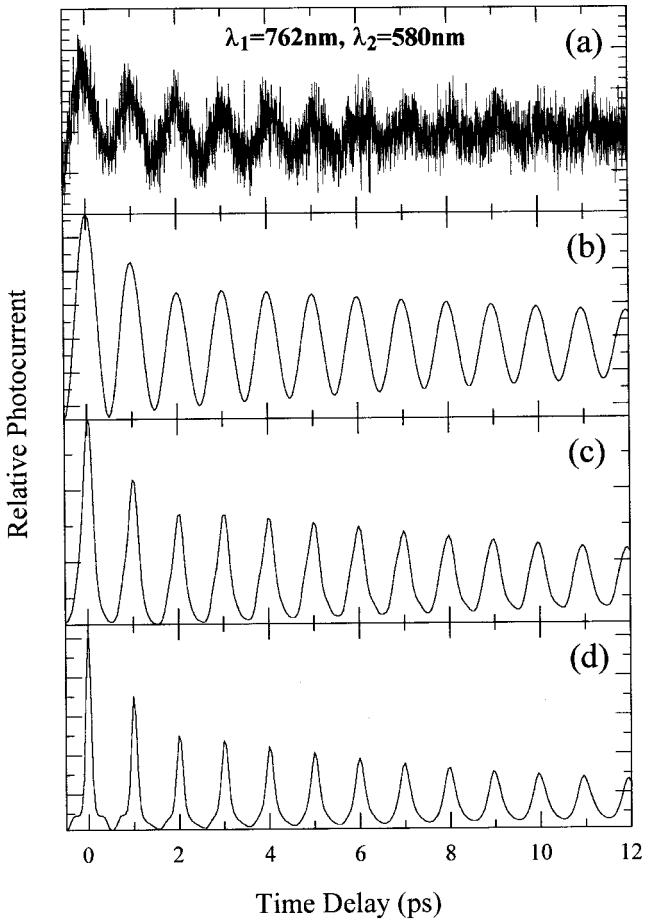

FIG. 10. Data (a) and calculated transients [(b)–(d)] similar to those of Fig. 9 but for $\lambda_1=762$ nm and $\lambda_2=580$ nm.

$(\Delta v=2)$ and higher harmonic frequency components are suppressed with respect to the fundamental [Fig. 11(c) and (g)].

The fact that including a positive linear chirp into the wave packet simulations is necessary to explain the data is gratifying since normal dispersion $(n''(\lambda)>0)$ in conventional optical elements produces positive chirp at the leading edge of a transform-limited pulse. Furthermore, self-phase modulation, the driving mechanism of continuum generation, produces a nonlinear chirp that can be approximated as a positive linear chirp.[34] It is interesting to note that if the sign of the chirp is reversed, the simulated transients are more narrow than those resulting from not considering chirp at all.

Therefore, improvement in the simulation of experiments is achieved by incorporating $|\Delta v|>1$ coherences and laser chirp into the calculations and, to our knowledge, these are the first simulations to do so. Considering higher-order contributions to the laser chirp may well improve further the agreement between theory and experiment. However, the gains are modest and, in the absence of detailed measurements of laser pulse phase, most aspects of the wave packet transient's frequency and temporal characteristics are described adequately by including only $\Delta v=\pm 1$ coherences.

C. Wave packets in the $D\,^1\Sigma_u^+$ state

The $D\,^1\Sigma_u^+$ state of Cs_2 has been studied extensively by several high resolution laser spectroscopic techniques, including Fourier transform spectroscopy and Doppler-free polarization spectroscopy.[18,20–23] As noted earlier, $D\,^1\Sigma_u^+$ vibrational levels above $v'\approx 30$ are perturbed by the bound $2\,^3\Pi_{ou}$ level and energy shifts exceeding 0.1 cm^{-1} were measured by Kâto *et al.*[22] for 14 $D\,^1\Sigma_u^+$ vibrational states in the $30\leqslant v'\leqslant 58$ interval. Predissociation of $D\,^1\Sigma_u^+$ also occurs through two mechanisms: spin-orbit interaction with $2\,^3\Pi_{ou}$, and L-uncoupling between the $2\,^3\Pi_{ou}$ state and the repulsive $c\,^3\Sigma_u^+$ potential.

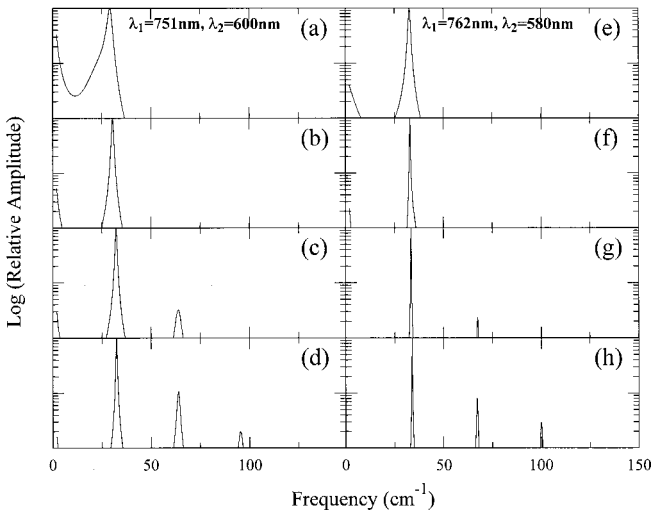

FIG. 11. Frequency spectra, calculated by the Maximum Entropy Method (Ref. 15), of the wavepacket signals of Fig. 9 [shown in panels (a)–(d) and those of Fig. 10 [right side, (e)–(h)]. Spectra (a) and (e) were calculated for 250 poles whereas the others involved adding a weak noise background (1% of the maximum signal value) to the theoretical transient and assuming 30 poles.

In calculating the $D-X$ FCFs shown in the upper portion of Fig. 12, the X state potential generated from the IPA data of Ref. 18 and the $D\,^1\Sigma_u^+$ state RKR potential of Ref. 22 (for $v'\leqslant 58$) as well as the $v'=59-65$ state energies of Ref. 23 were used. For higher vibrational states, the D state potential was approximated by the Morse function. The lower half of Fig. 12 displays the $D\leftarrow X$ absorption spectrum, calculated by weighting the FCFs with the X state vibrational state population distribution at $T=600$ K. Because of the large difference between R_e for the ground and D states $(\Delta R_e = R_{eD}[5.71\,\text{Å}$, Ref. 22$] - R_{eX}[4.65\,\text{Å}$, Refs. 18,27$]\cong 1\,\text{Å})$, maximum absorption occurs in the 570–580 nm region which arises predominantly from transitions to $v'\approx 30-50$ states. A comparison of the experimental photoelectron current-Δt scans for $\lambda_1=577$ nm and 600 nm with the results of numerical calculations are illustrated in Fig. 13. For vibrational wave packets composed of lower-lying D state vibrational levels, the simulations match the data reasonably well. When $\lambda_1=600$ nm, for example, $D\leftarrow X$ transitions populate predominantly $v'\approx 10-20$ states which are well-characterized and essentially free of perturbations. Near the peak of the $D\leftarrow X$ absorption band $(\lambda_1=577\,\text{nm})$, however, a discrepancy between the experimental curve and the theoretical prediction (upper panel, Fig. 13) becomes noticeable, presumably due to the involvement of $v'\gtrsim 40$ states.

In the frequency domain (cf. Fig. 14), the experimental

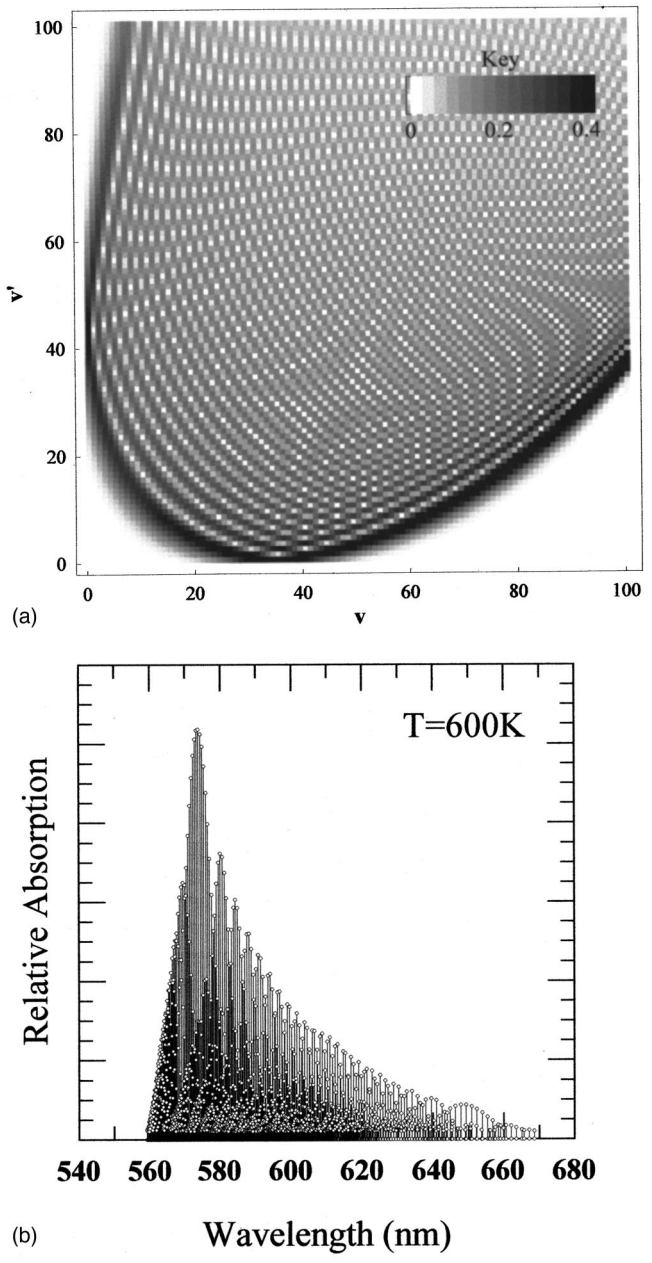

FIG. 12. Calculated $D-X$ Franck–Condon factors (top) and $D \leftarrow X$ absorption spectrum at 600 K.

and calculated wave packet transients for $\lambda_1 = 600$ nm are also in excellent agreement. The experimental profile is broader than the simulated version but otherwise the theory matches the data remarkably well. Both the peak at ~ 17.0 cm^{-1} and the weak pedestal lying at ~ 14 cm^{-1} are reproduced by the calculations. When $\lambda_1 = 577$ nm, on the other hand, the theoretical spectrum is shifted ~ 0.7 cm^{-1} to lower energy with respect to the experimental curve. This discrepancy appears to be directly attributable to the perturbation of the $D\,^1\Sigma_u^+$ state discussed earlier. The near reproduction of the experimental data by the simulations is actually remarkable when one considers that the D state wave packet is composed of a minimum of 20 vibrational states, and is a reflection of the precision of the experiments in Refs. 20–23 and 27.

IV. CONCLUSIONS

The temporal behavior of vibrational wave packets produced in the $B\,^1\Pi_u$ and $D\,^1\Sigma_u^+$ states of Cs_2 has been studied by pump–probe laser spectroscopy on the ~ 100 fs time scale. The $C\,^1\Pi_u$ state was chosen in Refs. 3 and 4 for initial experiments in this molecule for several reasons: (1) the large difference (~ 0.75 Å) between R_e for the C state relative to that for $Cs_2^+(X)$, which results in photoionization of $C\,^1\Pi_u$ in a narrow corridor near the classical inner turning points for the Cs_2^+ ($v^+ = 65-90$) vibrational levels[3] and a large modulation depth of the photoionization signal; (2) despite being weakly predissociated, $C\,^1\Pi_u$ is relatively unperturbed and has been thoroughly characterized by high resolution laser spectroscopy; and (3) the $C \leftarrow X$ transition is conveniently situated for excitation by a CPM system. In contrast, the equilibrium internuclear separations for the $B\,^1\Pi_u$ and $D\,^1\Sigma_u^+$ states differ from that for the Cs_2^+ ground state by ~ 0.38 Å and ~ 0.43 Å, respectively, or roughly half that for the C state. Also, $R_{eB} - R_e(Cs_2^+) < 0$ whereas $R_{eD} - R_e(Cs_2^+) > 0$. Consequently, the Cs_2 B and D states afford an opportunity to evaluate the wave packet detection approach introduced in Ref. 3—namely, monitoring the time and energy-integrated photoelectron current. As expected,

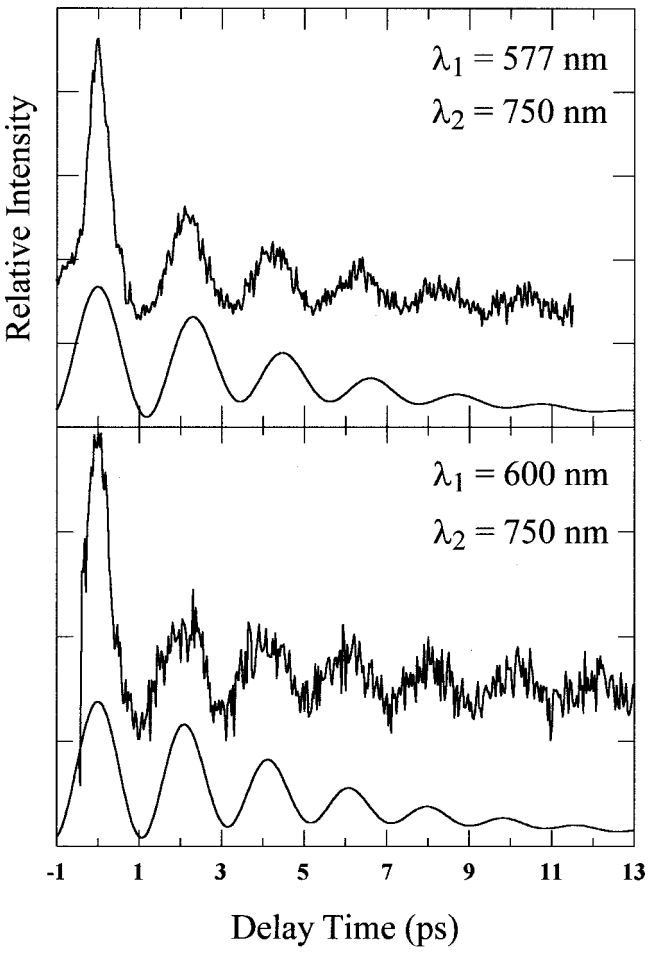

FIG. 13. Experimental and calculated traces of the relative photoelectron current as a function of time delay for vibrational wave packets in the $D\,^1\Sigma_u^+$ state and $\lambda_1 = 577$ nm and 600 nm. In both portions of the figure, $\lambda_2 = 750$ nm.

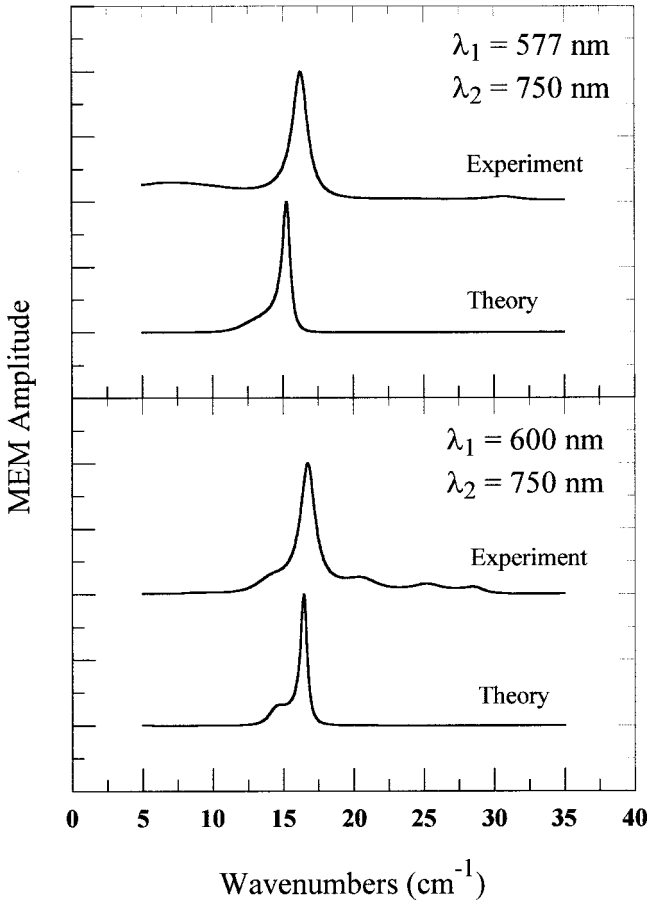

FIG. 14. Frequency domain representation of the experimental and simulated $D\,^1\Sigma_u^+$ wave packet transients of Fig. 13. Results are again shown for $\lambda_1 = 577$ and 600 nm for the probe central wavelength (λ_2) fixed at 750 nm. All spectra shown were calculated by the MEM approach, assuming 200 poles.

the smaller values for $|R_{eB,D} - R_e(Cs_2^+)|$ result in weaker modulation of the photoelectron current-Δt scans than was observed in the $C\,^1\Pi_u$ experiments but the S/N ratio is more than ample, suggesting that this experimental technique is applicable to a wider range of molecular transitions than originally anticipated.

By obtaining $B\,^1\Pi_u$ wave packet data for a range of pump and probe wavelengths and simulating the experimentally observed transients with the density matrix formalism (explicitly accounting for laser chirp), improved values for two spectroscopic constants have been determined: $R_e[Cs_2(B)] = 4.93 \pm 0.03$ Å and $T_e[Cs_2^+(X\,^2\Sigma_g^+)] = 29\,930 \pm 100\ cm^{-1}$. The underlying premise of this work is that evaluating simulated wave packet data with respect to several prominent characteristics (vibrational frequency, modulation depth, amplitude of the second harmonic relative to the fundamental, etc.) enables molecular constants to be determined or refined. Combining the experimental ability to vary λ_1 and λ_2 with computational analysis provides a powerful tool with which spectroscopic constants, measured originally in the frequency domain or, perhaps, as yet unknown, can be determined more precisely by analysis in the time domain.

The frequency composition of the D state vibrational wave packets is in accord with potentials and spectroscopic constants determined by laser spectroscopy in the frequency domain. It also appears that vibrational wave packets in the D state provide a tool for observing the $D\,^1\Sigma_u^+ - 2\,^3\Pi_{ou}$ interaction.

ACKNOWLEDGMENTS

The technical assistance of K. Collier and K. Kuehl is gratefully acknowledged. This work was supported by the U.S. Air Force Office of Scientific Research.

[1] T. Baumert, B. Bühler, R. Thalweiser, and G. Gerber, Phys. Rev. Lett. **64**, 733 (1990).
[2] T. Baumert, V. Engel, C. Röttgermann, W. T. Strunz, and G. Gerber, Chem. Phys. Lett. **191**, 639 (1992).
[3] G. Rodriguez and J. G. Eden, Chem. Phys. Lett. **205**, 371 (1993).
[4] G. Rodriguez, P. C. John, and J. G. Eden, J. Chem. Phys. **103**, 10473 (1995).
[5] V. Blanchet, M. A. Bouchène, O. Cabrol, and B. Girard, Chem. Phys. Lett. **233**, 491 (1995).
[6] V. Blanchet, M. A. Bouchène, and B. Girard, J. Chem. Phys. **108**, 4862 (1998).
[7] R. de Vivie-Riedle, B. Reischl, S. Rutz, and E. Schreiber, J. Phys. Chem. **99**, 16829 (1995).
[8] S. Rutz, R. de Vivie-Riedle, and E. Schreiber, Phys. Rev. A **54**, 306 (1996).
[9] J. M. Papanikolas, R. M. Williams, P. D. Kleiber, J. L. Hart, C. Brink, S. D. Price, and S. R. Leone, J. Chem. Phys. **103**, 7269 (1995).
[10] R. M. Williams, J. M. Papanikolas, J. Rathje, and S. R. Leone, J. Chem. Phys. **106**, 8310 (1997).
[11] T. S. Rose, M. J. Rosker, and A. H. Zewail, J. Chem. Phys. **88**, 6672 (1988).
[12] R. M. Bowman, M. Dantus, and A. H. Zewail, Chem. Phys. Lett. **161**, 297 (1989).
[13] M. Gruebele, G. Roberts, M. Dantus, R. M. Bowman, and A. H. Zewail, Chem. Phys. Lett. **166**, 459 (1990).
[14] V. Engel, Chem. Phys. Lett. **178**, 130 (1991).
[15] M. Gruebele and A. H. Zewail, J. Chem. Phys. **98**, 883 (1993).
[16] U. Diemer, R. Duchowicz, M. Ertel, E. Mehdizadeh, and W. Demtröder, Chem. Phys. Lett. **164**, 419 (1989).
[17] L. von Szentpály, Chem. Phys. Lett. **88**, 321 (1982).
[18] M. Raab, G. Höning, W. Demtröder, and C. R. Vidal, J. Chem. Phys. **76**, 4370 (1982).
[19] M. Raab, H. Weickenmeier, and W. Demtröder, Chem. Phys. Lett. **88**, 377 (1982).
[20] C. Amiot, W. Demtröder, and C. R. Vidal, J. Chem. Phys. **88**, 5265 (1988).
[21] K. Yokoyama, M. Baba, and H. Katô, J. Chem. Phys. **89**, 1209 (1988).
[22] H. Katô, T. Kobayashi, M. Chosa, T. Nakahori, T. Iida, S. Kasahara, and M. Baba, J. Chem. Phys. **94**, 2600 (1991).
[23] T. Kobayashi, T. Usui, T. Kamauchi, M. Baba, K. Ishikawa, and H. Katô, J. Chem. Phys. **98**, 2670 (1993).
[24] P. Kusch and M. M. Hessel, J. Mol. Spectrosc. **32**, 181 (1969).
[25] H. Katô and K. Yoshihara, J. Chem. Phys. **71**, 1585 (1979).
[26] C. R. Vidal and H. Scheingraber, J. Mol. Spectrosc. **65**, 46 (1977).
[27] W. Weickenmeier, U. Diemer, M. Wahl, M. Raab, W. Demtröder, and W. Müller, J. Chem. Phys. **82**, 5354 (1985).
[28] L. von Szentpály, P. Fuentealba, H. Preuss, and H. Stoll, Chem. Phys. Lett. **93**, 555 (1982).
[29] G. H. Jeung, J. P. Malrieu, and J. P. Daudey, J. Chem. Phys. **77**, 3571 (1982).
[30] M. Krauss and W. J. Stevens, J. Chem. Phys. **93**, 4236 (1990).
[31] M. Braun, C. Meier, and V. Engel, J. Chem. Phys. **103**, 7907 (1995).
[32] H. Helm and R. Möller, Phys. Rev. A **27**, 2493 (1983).
[33] G. H. Jeung, F. Spiegelmann, J. P. Daudey, and J. P. Malrieu, J. Phys. B **16**, 2659 (1983).
[34] See, for example, Q. Z. Wang, P. P. Ho, and R. R. Alfano, in *The Supercontinuum Laser Source*, edited by R. R. Alfano (Springer-Verlag, New York, 1989), p. 38.